AAS 08-298

OPTIMIZING PERIAPSIS-RAISE MANEUVERS USING LOW-THRUST PROPULSION

Brenton J. Duffy* **and David F. Chichka†**

This study considers the optimal control problem of maximizing the raise in the periapsis of a spacecraft orbit using continuous variable low-thrust propulsion. The dynamics of the spacecraft in the two-body system are modeled using Lagrange's planetary equations with the classic orbit elements as the state variables. Control is provided via the propulsion thrust components in the radial and circumferential directions. In addition, interior and terminal state constraints are considered to maintain the orbit apoapsis at a fixed altitude.

The problem is formally presented as a classic continuous optimal control problem subject to terminal and interior state constraints. The necessary conditions for optimality are derived including Pontryagin's minimum principle and the Legendre-Clebsch condition. The necessary conditions yield a multi-point boundary value problem, which is solved using the variation of extremals method. The results are presented for two cases where one enforces the apoapsis state constraints and the other does not. Both single orbit and multiple orbit maneuvers are considered.

The results show a trade-off between adding energy to the orbit via the semi-major axis according to the linearized vis-viva equation and circularizing the orbit by raising the periapsis and lowering the eccentricity. By comparing the low-thrust performance to equivalent impulsive maneuvers, the results demonstrate that the low-thrust systems can provide improved performance over the impulses in both the unconstrained and constrained cases. Furthermore, the efficiency of the low-thrust maneuver improves as more orbits are included in the maneuver as demonstrated by comparing normalized performance indices for the maximization of the periapsis.

For the unconstrained case, the trade-off between adding energy and circularizing causes significant variation in the optimal thrust profile between the orbits of a multiple orbit maneuver. The variation can be mitigated with some loss in performance by adding the interior apoapsis constraints to the optimization. This yields a uniform thrust profile over the entire maneuver, which is ideal for the design of optimized flight controllers.

INTRODUCTION

The inspiration for this study was derived from NASA's Magnetospheric Multiscale (MMS) mission set for launch in 2014. The primary goal of the MMS mission is to conduct scientific investigations of Earth's magnetosphere at altitudes ranging from 12 Earth radii up to 100 Earth radii.[1,2] The spacecraft must therefore be capable of performing frequent orbit-raising maneuvers and circularization maneuvers to maximize the time spent at the higher altitudes. This study focuses on the latter problem of circularizing the spacecraft orbit assuming an initial orbit that is highly eccentric.

The orbit circularization problem is formulated as a continuous optimal control problem for the variable low-thrust propulsion system using Lagrange's planetary equations to describe the system dynamics. An objective function is constructed that will maximize the performance of the circularization maneuver by maximizing the raise in periapsis while minimizing the fuel consumption. State constraints are also considered such that the apoapsis of the orbit is maintained at its initial altitude for specific points along the orbit. These state constraints are applied at interior points along the maneuver as well as at the end of the maneuver.

*Graduate Student, Department of Mechanical and Aerospace Engineering, The George Washington University, Staughton Hall 208, Washington, DC 20052.

†Assistant Professor of Engineering and Applied Science, Department of Mechanical and Aerospace Engineering, The George Washington University, Academic Center 726, Washington, DC 20052.

The resultant multi-point boundary value problem (MPBVP) is solved via the variations of extremals method for two cases, one where the apoapsis state constraints are not enforced and the other where they are enforced at every apoapsis pass and at the end of the maneuver.

Low-Thrust Propulsion

In the design of an exploration spacecraft, the performance of the propulsion system is usually the driving factor in the overall performance of the system. Since traditional systems use finite sets of impulsive burns, much control is lost during periods of coast. Low-thrust propulsion is one technology that has received increased interest in recent years as an alternative option to impulsive engines. These include such technologies as electric engines, solar sails, and laser systems, which are all characterized by continuous low-thrust. The potential advantages to such low-thrust propulsion systems include the ability to provide continuous and adaptive thrust control, which would provide access to regions of space and maneuver profiles that are difficult to achieve using impulsive maneuvers.

A great deal of work has already been done within the areas of low-thrust trajectory optimization. Notable contributions include the works of Jack H. Irving,[3] Theodore N. Edelbaum, et al.,[4,5,6,7] Jean A. Kechichian, et al.,[8,9,10,11] and many others. Irving considered the low-thrust problem in the late 1950s and included a derivation of the relationship between the optimal acceleration profile and the maximum payload capacity. He also considered the problems of low-thrust optimization in gravity-free space, in a central force field, and for a round trip mission to Mars. Edelbaum studied the problem of optimal low-thrust transfer trajectories in the 1960s and 70s and developed analytical results for certain assumptions by linearizing Lagrange's planetary equations about a circular orbit. In doing so, he developed the necessary optimal control laws to extremize any of the six classical orbit elements. He also developed solutions to the problem using equinoctial orbit elements, which is beneficial since it avoids the singularity issues associated with Lagrange's planetary equations. Since then, Kechichian has continued the work of Edelbaum and provided an excellent overview of the subject in Chobotov.[11] He further developed the use of equinoctial orbit elements in the optimization of the low-thrust trajectories as well as a slew of other element set formulations. By applying the methods of optimal control theory, Kechichian provided further insight into Edelbaum's problem of low-thrust transfer and derived solutions to other problems such as variable specific impulse, variable thrust, and minimizing transfer times. The works of Irving, Edelbaum, and Kechichian among others form much of the basis for the present study. In particular, the results derived by Edelbaum and Kechichian for optimizing the pure circularization maneuver are used as a source of comparison for the subsequent periapsis-raise circularization maneuver.

An important distinction must be noted between the circularization maneuvers considered by Edelbaum and Kechichian with those presented here. Edelbaum optimizes the circularization maneuver as an unconstrained maneuver to minimize the eccentricity.[7] Kechichian clarifies this problem and the resultant optimal control law by adding a state constraint such that the variation in the semi-major axis is zero thereby corresponding to pure circularization.[9,10] For this study, the circularization maneuver corresponds to the portion of an orbit-raise maneuver when the periapsis is raised in order to circularize at the apoapsis altitude. Thus, for this problem there will be variation in the semi-major axis and an increase in orbit energy so that the maneuver is not pure circularization. While the resultant control profiles and state trajectories certainly relate to the results from the problem studied by Edelbaum and Kechichian, the difference in the formulation of the problem and therefore the objective of the maneuver should be noted.

The aim of this study is not to necessarily develop new approaches to the problem of optimizing low-thrust trajectories. Instead, the focus is on applying the classical methods of optimal control theory specifically to the problem of optimally circularizing an eccentric orbit at the apoapsis altitude using low-thrust propulsion. The goal of the study is to use this problem to acquire greater insight into the dynamics of low-thrust trajectory optimization and how the system compares to traditional approaches using impulses.

OPTIMAL CONTROL THEORY FOR LOW-THRUST PROPULSION

Optimal Control Theory as it is applied for this study can be derived from the Calculus of Variations. It is used in the design of system controllers for optimizing a scalar performance index that is dependent on the control history and resultant state trajectories. The performance index can be any function that maps the system state space and control space to a scalar performance measure. Examples of common orbit maneuver performance indices include the transfer time, the total fuel consumption, or the total Δv. The optimal control problem is then solved by minimizing the performance index subject to the system dynamics and any state or control constraints.

Countless research has been conducted in the area of optimal control theory. The primary references used in this study include the texts by Arthur E. Bryson, et al.,[12] David F. Chichka,[13] David G. Hull,[14] and Donald E. Kirk.[15] The methods and derivations developed by these researchers are applied directly to the low-thrust optimization problem for circularizing an eccentric orbit while constraining the variation in the apoapsis altitude.

Problem Formulation

The low-thrust system dynamics are described using Lagrange's planetary equations, which are derived and discussed in detail in Bate, Mueller, and White[16] among others. Since the objective is to circularize the orbit, the maneuver need only be applied within the orbit plane of motion. Therefore, only three of the six Lagrange's planetary equations are necessary to describe the dynamics for in-plane, periapsis-raise maneuvers. These are listed in Eqs. 1–3. The element set includes the semi-major axis, the eccentricity, and the eccentric anomaly, which are represented as a, e, and E respectively. The applied acceleration is defined by the specific thrust components due to the low-thrust engine as expressed within the Euler-Hill frame. The symbols R and S represent the in-plane specific thrust components in the radial and circumferential directions respectively.

$$\frac{da}{dt} = \frac{2}{n}\left[\left(\frac{e\sin E}{1-e\cos E}\right)R + \left(\frac{\sqrt{1-e^2}}{1-e\cos E}\right)S\right] \tag{1}$$

$$\frac{de}{dt} = \frac{\sqrt{1-e^2}}{na}\left[\left(\frac{\sqrt{1-e^2}\sin E}{1-e\cos E}\right)R - \left(\frac{e-2\cos E+e\cos^2 E}{1-e\cos E}\right)S\right] \tag{2}$$

$$\begin{aligned}\frac{dE}{dt} = &\frac{1}{nae}\left[\left(\frac{-3e+(1+3e^2)\cos E - e^3\cos^2 E + e\sin^2 E}{(1-e\cos E)^2}\right)R\right.\\ &\left.+\left(\frac{-2+3e\cos E - e^2\cos^2 E}{(1-e\cos E)^2}\sqrt{1-e^2}\sin E\right)S\right] + \frac{n}{1-e\cos E}\end{aligned} \tag{3}$$

Note that the independent variable is time and is represented by t. In addition, n represents the mean motion of the spacecraft, which is defined as $n \equiv \sqrt{\mu/a^3}$. The last term on the right-hand side of Eq. 3 is the unperturbed variation in the eccentric anomaly due to the natural motion of the satellite while all of the other terms in Lagrange's planetary equations are due to the applied engine thrust.

The state variables are the three orbit elements of the semi-major axis, eccentricity, and eccentric anomaly and are represented by the state vector x as shown in Eq. 4. In addition, the control variables are the two in-plane specific thrust components, R and S, which are represented by the control vector u as shown in Eq. 5.

$$x = \left\{\begin{array}{ccc} a & e & E \end{array}\right\}^T \tag{4}$$

$$u = \left\{\begin{array}{cc} R & S \end{array}\right\}^T \tag{5}$$

The system dynamics are represented by the vector equation shown in Eq. 6 where the vector F represents all of terms on the right hand side of Eqs. 1–3 and the notation $\dot{x}$ represents the total time derivative of the states.

$$\dot{x} = F(x, u, t) \tag{6}$$

An objective function is defined to optimize the periapsis-raise maneuver by maximizing the resultant final raise in the periapsis radius as shown in Eq. 7. The variable ϕ represents the objective function to be minimized by the optimization. Note that the objective function is evaluated at the terminal state conditions at the end of the maneuver ($t = t_f$). A negative is included in the function so that when minimized it will maximize the final periapsis radius.

$$\phi(x(t_f)) = -a(t_f)\left[1 - e(t_f)\right] \tag{7}$$

As discussed in Bryson and Ho,[12] when the controls appear linearly in the dynamics as they do in Eqs. 1–3, the optimization will yield unbounded control. This means that unless the controls are constrained to some maximum and minimum values, the optimal control will fluctuate between zero and $\pm\infty$. This can be prevented directly by imposing limits on the controls using inequality constraints or alternatively by imposing a control-limiting penalty function. The latter method was chosen for this study so that trends could be studied in the variation of the thrust over the entire maneuver. Irving[3] derived an appropriate control penalty function as shown in Eq. 8, which when minimized will minimize the necessary fuel consumption of the maneuver.

$$L = \frac{k}{2}\left(R^2 + S^2\right) \tag{8}$$

By constructing the control penalty function is this fashion the specific thrust components are constrained via the scaling factor, k. The value of k will indirectly determine the maximum limit for the thrust magnitude by dictating the relative importance of minimizing the penalty function with respect to the primary objective function. A simple iterative routine is used to determine an appropriate value for k to bound the control within the desired limit.

The objective function and control penalty function are combined into one overall performance index J for the maneuver optimization as shown in Eq. 9.

$$\begin{aligned} J &= \phi(t_f) + \int_{t_0}^{t_f} L(x,u,t)dt \\ &= a(t_f)\left[e(t_f) - 1\right] + \int_{t_0}^{t_f} \frac{k}{2}\left(R^2 + S^2\right)dt \end{aligned} \tag{9}$$

In order to circularize the orbit, state constraints must be applied to limit the variation in the apoapsis radius. For missions interested in conducting scientific experiments at apoapsis, these state constraints are applied whenever the spacecraft passes apoapsis as well as at the end of the maneuver. This insures that at the end of the maneuver and during periods of scientific study, the apoapsis will remain at its initial value, but during other portions of the maneuver it is free to change. This approach necessitates the addition of a terminal constraint and a series of interior constraints applied whenever the spacecraft passes apoapsis where $E = (2n-1)\pi$ for $n = 1, 2, 3, ..., q$ and q is the number of constrained interior points. Note that for this study, a single orbit is defined as a revolution beginning and ending at periapsis, which means that the number of constrained interior points is equal to the number of orbits in the maneuver. The apoapsis interior constraints are defined as $\xi(x(t_n))$ as shown in Eq. 10 and the terminal constraint is defined as $\psi(x(t_f))$ as shown in Eq. 11.

$$\xi(x(t_n)) = \left\{ \begin{array}{c} a(t_n)\left[1 + e(t_n)\right] - r_s \\ E(t_n) - (2n-1)\pi \end{array} \right\} = 0 \tag{10}$$

for $n = 1, 2, 3, ..., q$ where q is the number of orbits

$$\psi(x(t_f)) = \left\{ \begin{array}{c} a(t_f)\left[1 + e(t_f)\right] - r_s \\ E(t_f) - E_f \end{array} \right\} = 0 \tag{11}$$

Using the performance index defined in Eq. 9 and the apoapsis constraints defined in Eqs. 10 and 11, the optimal control problem is formally posed as follows.

Minimize the performance index,

$$J = \phi(x(t_f)) + \int_{t_0}^{t_f} L(x,u,t)dt \tag{12}$$

subject to the dynamics

$$\dot{x} = F(x,u,t) \quad x(t_0) = x_0 \tag{13}$$

and the interior and terminal constraints

$$\xi(x(t_n)) = 0 \tag{14}$$

$$\psi(x(t_f)) = 0 \tag{15}$$

for $n = 1, 2, 3, ..., q$ where q is the number of orbits.

First-Order Necessary Conditions for Optimality

The derivation of the first- and second-order necessary conditions for an optimal maneuver trajectory can be performed using the classic methods of optimal control theory as discussed in the various optimal control texts included in the bibliography. For the inclusion of interior state constraints, the discussion in Chapter 3 of Bryson and Ho[12] was used as the basis for the following derivation.

The system dynamics are adjoined to the performance index using the Lagrange multipliers λ referred to as the co-states. In addition, the interior point constraints and terminal point constraint are adjoined using the constant multipliers η_n and ν respectively. Adjoining the dynamics and constraints in this way yields the augmented performance index shown in Eq. 16.

$$\begin{aligned}\tilde{J} = &\phi(x(t_f)) + \nu^T\psi(x(t_f)) + \eta_n^T\xi(x(t_n)) \\ &+ \int_{t_0}^{t_f} \left[L(x,u,t) + \lambda^T(t)F(x,u,t) - \lambda^T\dot{x}\right] dt\end{aligned} \tag{16}$$

The presence of the interior point constraints cause discontinuities to appear at $t = t_n$ in the otherwise continuous co-state functions. As such the integral in the augmented performance index must be split between each of the interior points using the limits t_n^- and t_n^+, which represent the times just before and after each t_n discontinuity.

$$\begin{aligned}\tilde{J} = &\phi(x(t_f)) + \nu^T\psi(x(t_f)) + \eta_n^T\xi(x(t_n)) \\ &+ \int_{t_0}^{t_1^-} \left[L(x,u,t) + \lambda^T(t)F(x,u,t) - \lambda^T(t)\dot{x}\right] dt \\ &+ \int_{t_n^+}^{t_{n+1}^-} \left[L(x,u,t) + \lambda^T(t)F(x,u,t) - \lambda^T(t)\dot{x}\right] dt \\ &+ \int_{t_q^+}^{t_f} \left[L(x,u,t) + \lambda^T(t)F(x,u,t) - \lambda^T(t)\dot{x}\right] dt\end{aligned} \tag{17}$$

The Hamiltonian function is defined in the usual manner as shown in Eq. 18.

$$H(x,u,\lambda,t) = L(x,u,t) + \lambda^T(t)F(x,u,t) \tag{18}$$

The first order necessary conditions are determined according to the variation in the augmented performance index due to variations in the control vector and free terminal and interior times. This is shown in Eq. 19.

$$
\begin{aligned}
\delta\tilde{J} \;=\;& \lambda^T(t_0)\delta x(t_0) \\
&+ \left[\frac{\partial\phi}{\partial x}(t_f) + \nu^T\frac{\partial\psi}{\partial x}(t_f) - \lambda^T(t_f)\right]\delta x(t_f) + \left[\frac{\partial\phi}{\partial t} + \nu^T\frac{\partial\psi}{\partial t} + H(t_f)\right]dt_f \\
&+ \left[\eta_n^T\frac{\partial\xi}{\partial x}(t_n) + \lambda^T(t_n^+) - \lambda^T(t_n^-)\right]dx(t_n) + \left[\eta_n^T\frac{\partial\xi}{\partial t}(t_n) - H(t_n^+) + H(t_n^-)\right]dt_n \\
&+ \int_{t_0}^{t_1^-}\left[\left(\frac{\partial H}{\partial x} + \dot{\lambda}^T\right)\delta x + \frac{\partial H}{\partial u}\delta u\right]dt + \int_{t_n^+}^{t_{n+1}^-}\left[\left(\frac{\partial H}{\partial x} + \dot{\lambda}^T\right)\delta x + \frac{\partial H}{\partial u}\delta u\right]dt \\
&+ \int_{t_q^+}^{t_f}\left[\left(\frac{\partial H}{\partial x} + \dot{\lambda}^T\right)\delta x + \frac{\partial H}{\partial u}\delta u\right]dt
\end{aligned} \tag{19}
$$

For an extremal solution the first variation of the augmented performance index must vanish, which dictates the first-order necessary conditions shown in Eqs. 20–27.

$$\dot{\lambda}^T = -\frac{\partial H}{\partial x} \tag{20}$$

$$\lambda^T(t_f) = \frac{\partial\phi}{\partial x}(t_f) + \nu^T\frac{\partial\psi}{\partial x}(t_f) \tag{21}$$

$$0 = \frac{\partial H}{\partial u} \tag{22}$$

$$0 = H(t_f) + \frac{\partial\phi}{\partial t}(t_f) + \nu^T\frac{\partial\psi}{\partial t}(t_f) \tag{23}$$

$$\psi(x(t_f)) = 0 \tag{24}$$

$$0 = \lambda^T(t_n^+) - \lambda^T(t_n^-) + \eta_n^T\frac{\partial\xi}{\partial x}(t_n) \tag{25}$$

$$0 = H(t_n^+) - H(t_n^-) - \eta_n^T\frac{\partial\xi}{\partial t}(t_n) \tag{26}$$

$$\xi(x(t_n)) = 0 \tag{27}$$

Note that Eqs. 20–24 represent the usual first-order necessary conditions for a free final time optimal control problem subject to a terminal constraint. In addition, Eqs. 25–27 are required due to the enforcement of the interior point constraints. Note that Eq. 25 defines the discontinuities in the co-states. However, since time does not explicitly appear in any of the system equations, the discontinuities in the Hamiltonian go to zero for the optimal control solution as evident in Eq. 26 when $\partial\xi/\partial t = 0$.

Pontryagin's Minimum Principle

Applying the weak form of Pontryagin's minimum principle from Eq. 22 to the low-thrust maneuver yields the optimal control laws shown in Eqs. 28 and 29 for the in-plane specific thrust components.

$$
\begin{aligned}
R = -\frac{1}{kn}\Bigg[&\frac{2e\sin E}{1-e\cos E}\lambda_1 + \frac{(1-e^2)\sin E}{a(1-e\cos E)}\lambda_2 \\
&+ \frac{-3e + (1+3e^2)\cos E - e^3\cos^2 E + e\sin^2 E}{ae(1-e\cos E)^2}\lambda_3\Bigg]
\end{aligned} \tag{28}
$$

$$
\begin{aligned}
S = -\frac{1}{kn}\Bigg[&\frac{2\sqrt{1-e^2}}{1-e\cos E}\lambda_1 - \frac{\sqrt{1-e^2}(e - 2\cos E + e\cos^2 E)}{a(1-e\cos E)}\lambda_2 \\
&- \frac{(2 - 3e\cos E + e^2\cos^2 E)\sqrt{1-e^2}\sin E}{ae(1-e\cos E)^2}\lambda_3\Bigg]
\end{aligned} \tag{29}
$$

Both of the control laws must be satisfied throughout the maneuver in order for the solution to be optimal. Notice that the specific thrust components are inversely proportional to the penalty function weighting factor, k, which means that to limit the engine to low-thrust, this factor must be large. In performing the numerical optimization, it is necessary to iteratively determine an appropriate value for the weighting factor such that the specific thrust magnitude is bound below the desired limit.

Legendre-Clebsch Condition

Once an extremal control history has been determined using Eqs. 28 and 29, to prove that it is a minimizing solution for the performance index, the Legendre-Clebsch condition must be satisfied. This condition is shown in Eq. 30.

$$\frac{\partial^2 H}{\partial u^2} = \begin{bmatrix} \frac{\partial^2 H}{\partial R^2} & \frac{\partial^2 H}{\partial R \partial S} \\ \frac{\partial^2 H}{\partial S \partial R} & \frac{\partial^2 H}{\partial S^2} \end{bmatrix} \geq 0 \tag{30}$$

The Legendre-Clebsch condition states that in order for the extremal control to be minimizing, the matrix of second-order partial derivatives for the Hamiltonian function with respect to the control vector must be positive semi-definite. Since the only quadratic control terms that appear in the Hamiltonian function are from the penalty function, Eq. 8, the resultant Legendre-Clebsch matrix is entirely a function of the penalty function weighting factor, k as shown in Eq. 31.

$$\frac{\partial^2 H}{\partial u^2} = \begin{bmatrix} k & 0 \\ 0 & k \end{bmatrix} \geq 0 \tag{31}$$

Thus, to insure that the extremal control is a minimizer of the performance index one need only choose a positive value for k. If a negative term were used, the control would be a maximizer and if zero were chosen, the solution would be unbounded. For this study, k is chosen as a large positive value in order for the extremal control to be the minimizing control.

NUMERICAL SOLUTIONS

The first-order necessary conditions for the multi-orbit optimal low-thrust maneuver were derived and presented in Eqs. 20–27. In conjunction with the system dynamics listed in Eqs. 1–3 and the initial state conditions, the necessary conditions for optimality yield a multi-point boundary value problem (MPBVP) for the optimal control history and resultant state trajectory. The MPBVP is solved using the variation of extremals method, also known as the shooting method. It solves the problem by integrating the differential equations using guessed values for the free variables including the initial and interior point values for the co-states, $\lambda(t_0)$ and $\lambda(t_n^+)$, and all of the constant constraint multipliers, η_n and ν. The state and co-state differential equations are integrated using these guessed values and the results are used to iteratively determine the correct values that satisfy all of the interior and terminal conditions of optimality.

There are a multitude of approaches used to implement the variations of extremals method. Breakwell, Speyer, and Bryson[17] present a useful approach for converging the variation of extremals method for a two-point boundary value problem (TPBVP). Their methodology is extended for the case of the MPBVP by incorporating the interior constraints.

In order, to execute the numerical studies, values must be assigned to the input design parameters of the optimization. These include the initial state conditions for the orbit, the prescribed values for the interior eccentric anomalies, which implicitly define the interior times, t_n, and the maximum limit imposed on the thrust magnitude. In addition, the number of orbits of the maneuver must be defined, which for this study will include the cases of a single orbit, five orbits, ten orbits, and fifteen orbits. All of the optimization parameters are listed in Eqs. 32.

$$
\begin{aligned}
&a(t_0) = 7 \text{ AU} \quad e(t_0) = 0.707 \\
&r_a(t_0) = 12 \text{ AU} \quad r_p(t_0) = 2 \text{ AU} \\
&E(t_0) = 0 \quad E(t_f) = (2\pi)q \quad E(t_n) = (2n-1)\pi \\
&\sqrt{R^2 + S^2} \leq 0.5 \text{ mm/s}^2
\end{aligned} \tag{32}
$$

$$\text{for } n = 1, 2, 3, ..., q \text{ and } q = 1, 5, 10, 15$$

Unconstrained Apoapsis Maneuver

As an initial case, the optimization is simplified by neglecting the interior and terminal apoapsis state constraints, which means there are no constraint multipliers, η_n or ν and Eqs. 24–27 are no longer necessary. As such, the maneuver no longer corresponds directly to a circularization at the initial apoapsis altitude, but rather to the maneuver for maximizing the raise in periapsis without regard to the variation in the apoapsis. The results from this case will serve as a basis of comparison for the next case where the apoapsis state constraints are enforced. The results from the unconstrained variation maneuver are presented graphically in Appendix A.

Figures 1–4 show the variation in the orbit elements including the semi-major axis, eccentricity, and apsidal radii as plotted with respect to the eccentric anomaly rather than time. The increase in the periapsis radius and decrease in the eccentricity demonstrate that the orbit is being circularized, but not to any prescribed altitude. Since there are no constraints on the apoapsis, the optimization is free to increase it as much as necessary to maximize the periapsis. This causes significant variation in the apoapsis radius and semi-major axis corresponding to a significant increase in orbit energy.

Note that as the number of orbits increases the secular terms tend to dominate over the cyclical terms and the variations become approximately linear with respect to the eccentric anomaly. This is evident in each of the four element plot sets. Such results support the approach taken by Edelbaum[7] who linearized the dynamic equations of motion with respect to a circular orbit to represent maneuvers spanning many orbits.

The specific thrust profiles for the unconstrained maneuvers are shown in Figure 5 and the thrust directions as measured with respect to the local horizontal are shown in Figure 6. Notice that the thrust profile is not uniform across all of the maneuver orbits, but changes depending on the number of orbits included in the maneuver. In general, the thrust is maximized and directed tangential to the orbit at apoapsis, corresponding to the optimal location for a periapsis-raising impulsive burn. However, there is significant nonzero thrust components applied at periapsis as well, which increases as more orbits are included, but decreases as the maneuver progresses. This phenomenon is related to the inherent trade-off occurring in the optimization between adding energy to the orbit by thrusting at periapsis and using the energy to raise periapsis by thrusting at apoapsis. Since no constraints are enforced on the apoapsis, the optimization is free to raise it as much as necessary to raise the orbit energy and maximize the raise in periapsis.

The orbit trajectories for the unconstrained case are shown in Figure 7. For the sake of clarity the trajectories are plotted within a reference frame that is fixed to the orbit line of apsides, which has a small secular rotation with respect to the inertial frame due to the variation in the argument of periapsis. The orbit trajectories demonstrate that the maneuver increases the orbit size and decreases its eccentricity toward circularization.

Constrained Apoapsis Maneuver

The second set of optimized maneuvers apply to the low-thrust periapsis-raise problem with apoapsis constraints at the end of the maneuver and at each apoapsis pass. The terminal constraint in Eq. 11 is included to insure that the final orbit apoapsis is at the desired altitude. In addition, the interior constraints of Eqs. 10 are enforced at every apoapsis pass as discussed previously. The added constraints cause discontinuities to

appear in all of the co-state profiles, but not in the Hamiltonian functions since this problem has no explicit time dependencies. The results for the constrained apoapsis maneuver over single and multiple orbits are presented graphically in Appendix B.

Figures 8–11 show the variation in the orbit elements including the semi-major axis, eccentricity, and apsidal radii. The added terminal constraint on the apoapsis forces the final variation in the apoapsis to equal zero. In addition, within every orbit the apoapsis and semi-major axis cyclically decrease and increase such that the apoapsis variation is zero at each apoapsis pass. All the while, the periapsis radius is increasing and the eccentricity decreasing toward circularization. Thus, even though the maneuver must limit the increase in orbit energy to meet the interior and terminal constraints, it is still optimally directing the thrust to maximize the final periapsis radius. The total variation in the elements are smaller than in the unconstrained maneuver because energy must be diverted toward satisfying the apoapsis state constraints.

The specific thrust profile and thrust direction are shown in Figures 12–13 with respect to the eccentric anomaly. Notice that in this case the results closely resemble those derived by Edelbaum[7] and Kechichian[9,10] for the unconstrained minimization of the orbit eccentricity. The thrust is maximized at apoapsis and is directed approximately perpendicular to the line of apsides. The thrust is also non-zero at periapsis as it was in the unconstrained case. However, in this case the periapsis thrust is directed opposite to the velocity vector, which causes the apoapsis to decrease. This is necessary in order to satisfy the apoapsis state constraints appearing later in the maneuver. Note also that the thrust profile is uniform across all of the orbits for the constrained maneuver. Therefore, the control profile derived for the single orbit case is readily applied to the maneuver as a whole regardless of the number of orbits.

The transfer trajectories for each constrained maneuver are shown in Figure 14 within a rotating reference frame that is fixed to the orbit line of apsides. It is apparent that the variation in the apoapsis has been constrained such that it is always close to zero, while the periapsis increases with each successive orbit.

CONCLUSION

The optimization of the low-thrust periapsis-raise maneuver with apoapsis constraints was conducted using the variation of extremals method yielding the optimal thrust profiles and resultant transfer trajectories shown in the Appendices. The method was applied for both single and multi-orbit maneuvers using two formulations: unconstrained apoapsis, and interiorly and terminally constrained apoapsis.

The resultant change in the orbit elements for each of the low-thrust maneuvers and for all of the optimization schemes are tabulated in Table 1. The objective of the maneuver was to maximize the periapsis radius in order to circularize the orbit. However, note that while the periapsis was raised more in the unconstrained cases than in the constrained cases, the resultant change in the orbit eccentricity was less. Thus, the latter case is more closely related to the pure circularization maneuver.

Table 1 Variation in the Orbit Elements

Objective	$\%\Delta a$	$\%\Delta e$	$\%\Delta r_p$	$\%\Delta r_a$
Unconstrained Single Orbit Maneuver	1.19	-1.71	5.37	0.48
Unconstrained Five Orbit Maneuver	7.78	-9.00	31.19	3.77
Unconstrained Ten Orbit Maneuver	20.13	-17.96	72.20	11.19
Unconstrained Fifteen Orbit Maneuver	35.43	-25.70	119.44	21.02
Constrained Single Orbit Maneuver	0.76	-1.81	5.17	0.00
Constrained Five Orbit Maneuver	4.11	-9.53	28.04	0.00
Constrained Ten Orbit Maneuver	9.15	-20.24	62.45	0.00
Constrained Fifteen Orbit Maneuver	15.41	-32.23	105.17	0.00

To interpret the resultant trade-off between thrusting to increase the orbit energy and thrusting directly to

raise the periapsis, consider the linearized vis-viva equation shown in Eq. 33. This equation relates the change in orbit energy due to an applied change in the instantaneous velocity and/or position. While instantaneously changing the position is not possible, instantaneous velocity changes are possible through Δv impulses.

$$\Delta\mathcal{E} = v\Delta v + \frac{\mu}{r^2}\Delta r \tag{33}$$

Notice that the change in the orbit energy is proportional to the applied Δv according to the velocity of the spacecraft during the impulse. Therefore, to maximize the change in the orbit energy, the impulse should be applied whenever the orbit velocity is at its greatest, which for elliptic orbits is at periapsis. However, the optimal location to raise periapsis is to burn at apoapsis. Therefore, for continuous maneuvers the optimal thrust profile will be a combination of both whereby thrusting at periapsis raises the orbit energy, which improves the efficiency of the maneuver, and thrusting at apoapsis directly raises the periapsis radius. This clarifies why the optimal thrust profiles included non-zero thrust components at periapsis yielding cyclical variations in the apoapsis and semi-major axis.

Low-Thrust Maneuver vs. Impulsive Maneuver

The results from all of the cases for the resultant low-thrust propulsion maneuvers will now be compared to an equivalent maneuver using one or more impulses from high-thrust engines. The performance measures include the total Δv according to the Eq. 34 and the mass ratio according to Eq. 35. The mass ratio is defined as the final spacecraft mass over the initial mass, which is a measure of the payload capacity. The performance measures are tabulated for each case in Table 2 along with the corresponding change in the periapsis radius. The specific impulses of the propulsion systems are defined using typical values for each of 300 seconds and 1500 seconds respectively.

$$\Delta v = \int_{t_0}^{t_f} \sqrt{R^2 + S^2}dt \tag{34}$$

$$MR = e^{-\Delta v/(I_{sp}g_0)} \tag{35}$$

Table 2 Performance Results

		Impulse $I_{sp} = 300$ s		Low-Thrust $I_{sp} = 1500$ s	
Objective	Δr_p (AU)	Δv (m/s)	MR	Δv (m/s)	MR
Unconstrained Single Orbit Maneuver	0.11	30.16	0.986	33.85	0.998
Unconstrained Five Orbit Maneuver	0.64	163.44	0.946	183.32	0.988
Unconstrained Ten Orbit Maneuver	1.49	336.97	0.892	383.08	0.974
Unconstrained Fifteen Orbit Maneuver	2.46	488.66	0.847	567.53	0.962
Constrained Single Orbit Maneuver	0.11	26.75	0.991	33.32	0.998
Constrained Five Orbit Maneuver	0.58	134.63	0.955	168.31	0.987
Constrained Ten Orbit Maneuver	1.29	271.73	0.912	341.41	0.977
Constrained Fifteen Orbit Maneuver	2.17	411.75	0.869	520.29	0.965

In terms of performance, the low-thrust maneuvers all required more Δv than an equivalent maneuver using impulses. However, due to the high specific impulse of low-thrust engines, the resultant mass ratios were all higher than for the impulsive alternative. A higher mass ratio means that less propellant mass is required and consequently there is more payload mass available. Thus, one conclusion that can be drawn from this study is that a low-thrust engine with a specific impulse of 1500 seconds and a maximum thrust capacity of 0.5 $\mathrm{mm/s^2}$ can outperform a standard impulsive system with a specific impulse of 300 seconds.

Dependence on Number of Orbits

Another important phenomenon that was discovered for low-thrust maneuver optimization is the dependence on the number of orbits. For the unconstrained maneuvers, the optimal control history and resultant trajectories for each orbit changed depending on the total number of orbits in the maneuver. The early orbits in the maneuver focused their thrusting toward adding energy to the system by raising apoapsis, while the later orbits converted all of their thrust and the orbit's energy toward raising periapsis and lowering the eccentricity. This again relates to the linearized vis-viva equation shown in Eq. 33. In contrast, the maneuver with apoapsis constraints applied to each orbit had thrust profiles that were uniform across all of the orbits. This means that one could optimize the thrust over a single orbit and apply the results to the entire maneuver and it would still be optimal.

In comparing the performance between the unconstrained and constrained maneuvers, it became apparent that adding apoapsis constraints to the system decreases the optimal performance capabilities of the maneuver. To gain a better understanding of the efficiency of the maneuvers and possible losses due to the additional constraints, consider the following normalized performance indices tabulated in Table 3. The first is defined by the ratio of the resultant change in the periapsis, $\%\Delta r_p$, over the necessary Δv. In addition, to evaluate the performance dependence on the number of orbits, the second normalized performance index is defined as the ratio of the change in periapsis, $\%\Delta r_p$, over q, the number of orbits.

Table 3 Normalized Performance Results

Objective	$\%\Delta r_p/\Delta v$	$\%\Delta r_p/q$
Unconstrained Single Orbit Maneuver	0.159	5.37
Unconstrained Five Orbit Maneuver	0.170	6.24
Unconstrained Ten Orbit Maneuver	0.188	7.22
Unconstrained Fifteen Orbit Maneuver	0.210	7.96
Constrained Single Orbit Maneuver	0.155	5.17
Constrained Five Orbit Maneuver	0.167	5.61
Constrained Ten Orbit Maneuver	0.183	6.25
Constrained Fifteen Orbit Maneuver	0.202	7.01

Examining these results, a number of interesting observations can be made. First, notice that both performance index ratios increase as the number of orbits increases. Higher ratios means more change in the periapsis radius per unit Δv or per orbit, which is more efficient. Therefore, the efficiency of the low-thrust maneuver increases as the number of orbits increases.

Another important observation is that there is some loss due to the inclusion of apoapsis constraints as evident in the smaller ratios for the constrained cases. However, these losses are relatively small. Recall that interiorly constrained maneuvers yield thrust profiles that are uniform across all of the orbits, which was not true for the unconstrained case. In terms of mission planning and controller design, it is desirable to be able to derive the optimal control laws using a single orbit and then apply those control laws to the entire maneuver over any number of orbits. However, this is only optimal for the interiorly constrained case, which showed some loss in efficiency as compared to the unconstrained case. Nonetheless, the loss was small and it may prove more beneficial to accept these losses so that the control law is the same for all orbits, which greatly simplifies the design of the spacecraft controller.

REFERENCES

[1] D. Smith, "Solar Terrestial Probes Magnetospheric Multiscale Mission," Dec. 3 2007. <http://stp.gsfc.nasa.gov/missions/mms/mms.htm>, Site accessed on May 9, 2008,.

[2] A. S. Sharma and S. A. Curtis, *Nonequilibrium Phenomena in Plasmas*, ch. Magnetospheric Multiscale Mission: Cross-scale Exploration of Complexity in the Magnetosphere, pp. 179–195. The Netherlands: Springer, 2005.

[3] J. H. Irving, *Space Technology*, ch. 10, "Low thrust Flight: Variable Exhaust Velocity in Gravitational Fields". New York: John Wiley and Sons, 1959.

[4] T. N. Edelbaum, W. R. Fimple, F. W. Gobetz, and H. S. London, "Applications of Ion Propulsion to NASA Missions," *ARS Space Flight Report to the Nation*, 1961.

[5] T. N. Edelbaum, "The Use of High- and Low-Thrust Propulsion in Combination for Space Missions," *Journal of the Astronautical Sciences*, Vol. 9, 1962, pp. 49–60.

[6] T. N. Edelbaum, "Optimum low-thrust transfer between circular and elliptic orbits," *Proceedings of the Fourth U.S. National Congress of Applied Mechanics*, New York, American Society of Mechanical Engineers, 1962, pp. 137–141.

[7] T. N. Edelbaum, "Optimum Low-Thrust Rendezvous and Station Keeping," *AIAA Journal*, Vol. 2, July, pp. 1196–1201.

[8] J. A. Kechichian, "Reformulation of Edelbaum's Low-Thrust Transfer Problem Using Optimal Control Theory," *Journal of Guidance, Control, and Dynamics*, Vol. 20, No. 5, 1997, pp. 988–994.

[9] J. A. Kechichian, "Low-Thrust Eccentricity-Constrained Orbit Raising," *Journal of Spacecraft and Rockets*, Vol. 35, No. 3, 1998, pp. 327–335.

[10] J. A. Kechichian, "Constrained Circularization in Elliptic Orbits Using Low Thrust with Shadowing Effect," *Journal of Guidance, Control, and Dynamics*, Vol. 26, No. 6, 2003, pp. 949–955.

[11] J. A. Kechichian, *Orbital Mechanics*, ch. 14, "Optimal Low-Thrust Orbit Transfer", pp. 335–410. Reston, VA: American Institute of Aeronautics and Astronautics, Inc., 2002.

[12] A. E. Bryson and Y.-C. Ho, *Applied Optimal Control Theory*. Waltham, Massachusetts: Blaisdell Publishing Company, 1969.

[13] D. F. Chichka, "Optimal Control Theory for Scientists and Engineers," Lecture Notes on Electromechanical Control Systems, The Department of Mechanical and Aerospace Engineering, The George Washington University, 2008.

[14] D. G. Hull, *Optimal Control Theory for Applications*. New York: Springer, 2003.

[15] D. E. Kirk, *Optimal Control Theory*. New York: Dover, 1998.

[16] R. R. Bate, D. D. Mueller, and J. E. White, *Fundamentals of Astrodynamics*. New York: Dover, 1971.

[17] J. V. Breakwell, J. L. Speyer, and A. E. Bryson, "Optimization and Control of Nonlinear Systems using the Second Variation," *SIAM Journal of Control*, Vol. 1, No. 2, 1963, pp. 193–223.

APPENDIX A: UNCONSTRAINED APOAPSIS MANEUVER RESULTS

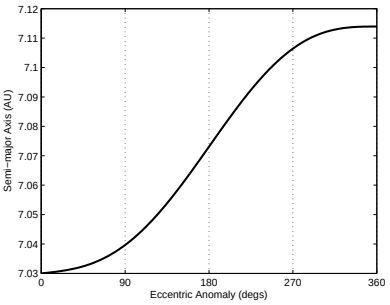

(a) One Orbit

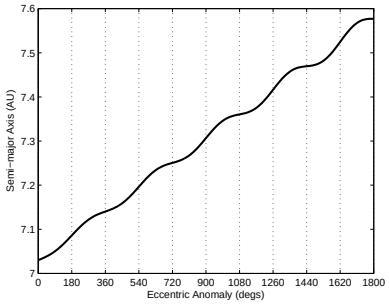

(b) Five Orbits

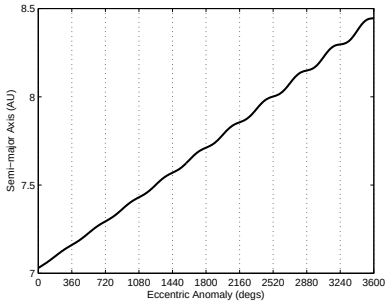

(c) Ten Orbits

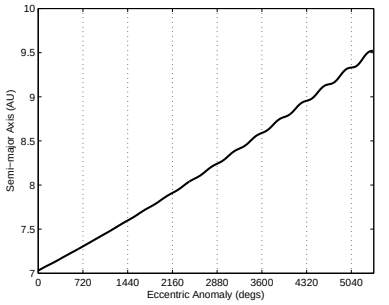

(d) Fifteen Orbits

Figure 1 Semi-Major Axis for Unconstrained Apoapsis Maneuver

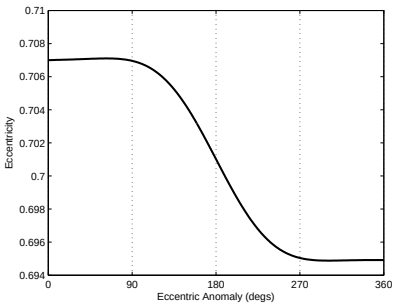

(a) One Orbit

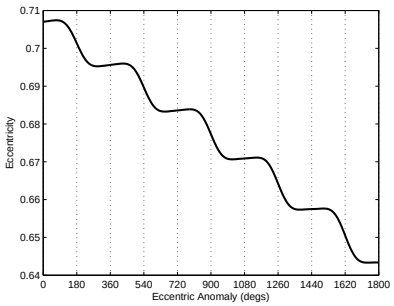

(b) Five Orbits

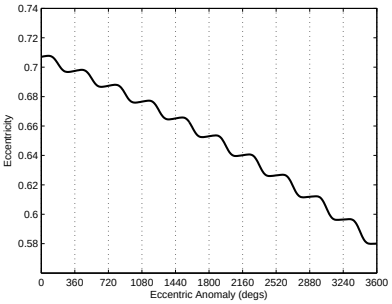

(c) Ten Orbits

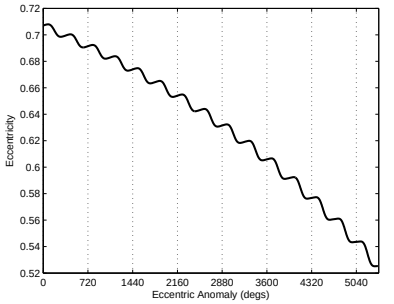

(d) Fifteen Orbits

Figure 2 Eccentricity for Unconstrained Apoapsis Maneuver

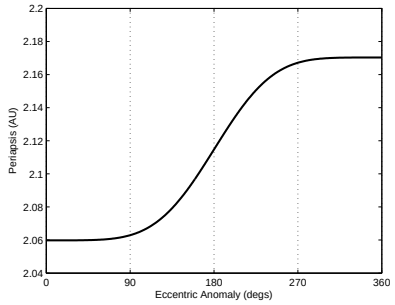

(a) One Orbit

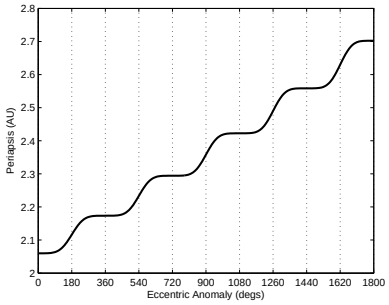

(b) Five Orbits

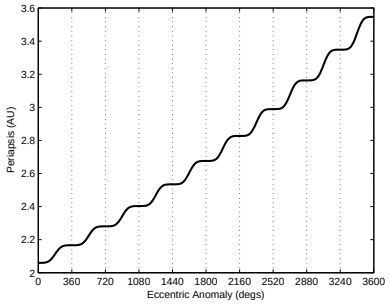

(c) Ten Orbits

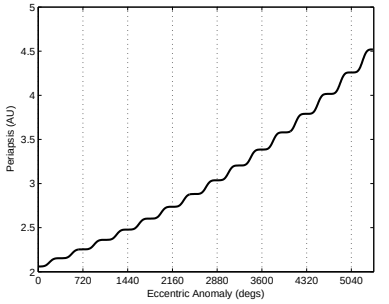

(d) Fifteen Orbits

Figure 3 Periapsis Radius for Unconstrained Apoapsis Maneuver

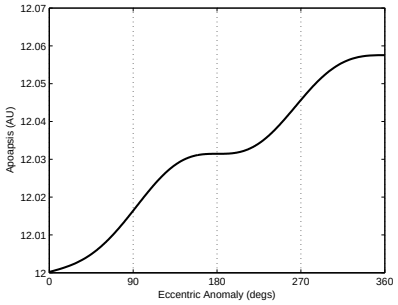

(a) One Orbit

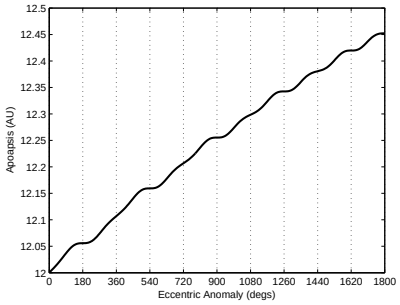

(b) Five Orbits

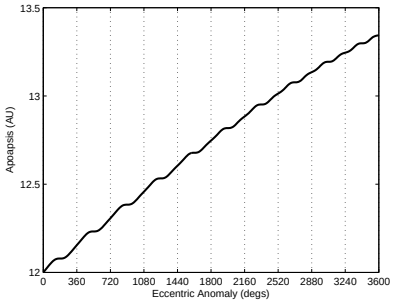

(c) Ten Orbits

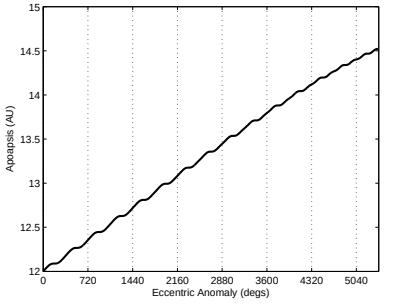

(d) Fifteen Orbits

Figure 4 Apoapsis Radius for Unconstrained Apoapsis Maneuver

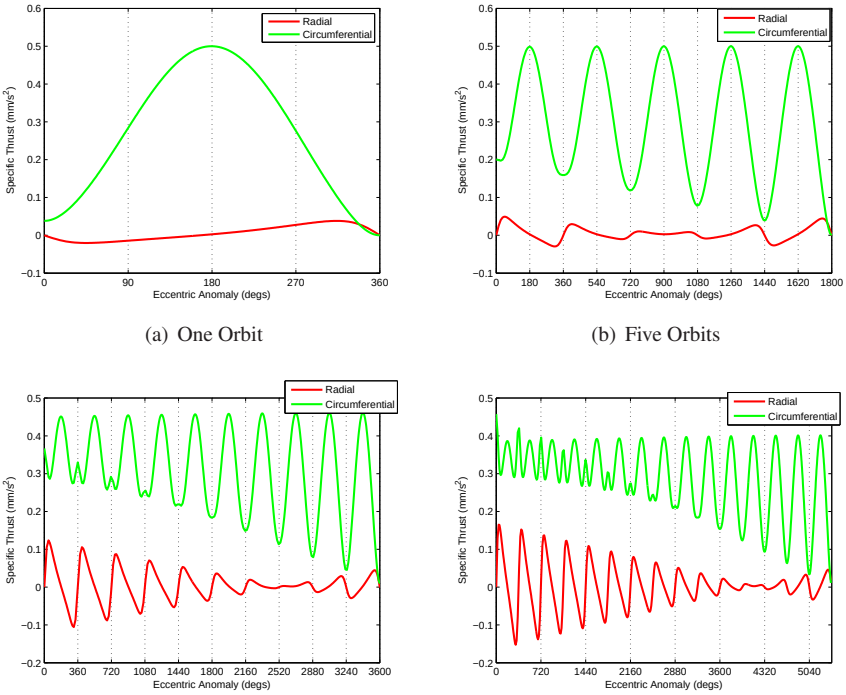

(a) One Orbit (b) Five Orbits

(c) Ten Orbits (d) Fifteen Orbits

Figure 5 Specific Thrust for Unconstrained Apoapsis Maneuver

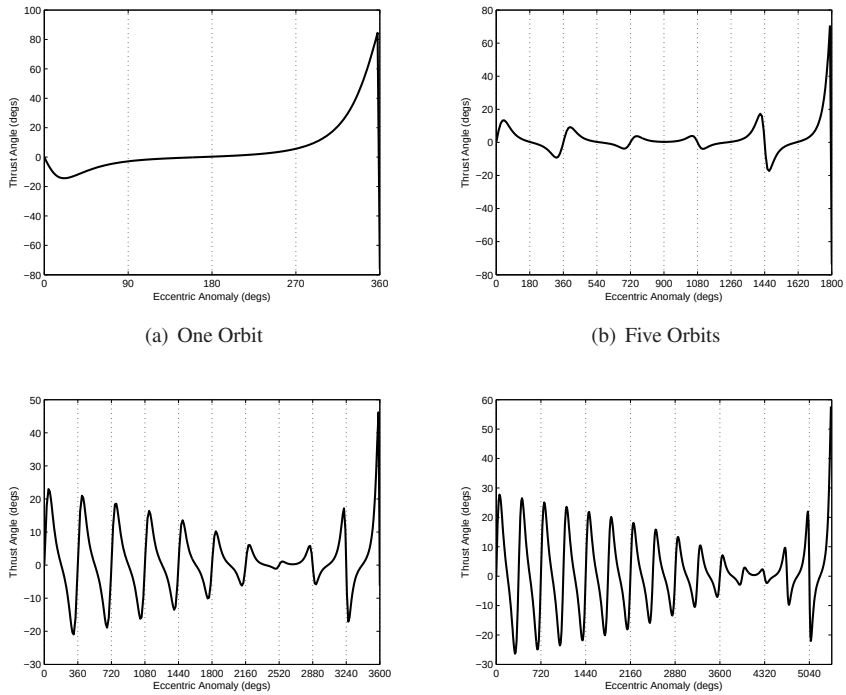

(a) One Orbit (b) Five Orbits

(c) Ten Orbits (d) Fifteen Orbits

Figure 6 Thrust Direction for Unconstrained Apoapsis Maneuver

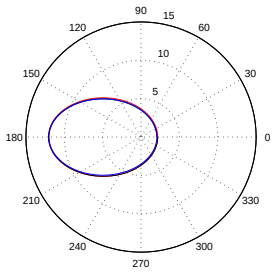

(a) One Orbit

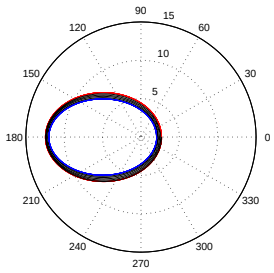

(b) Five Orbits

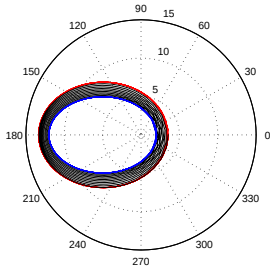

(c) Ten Orbits

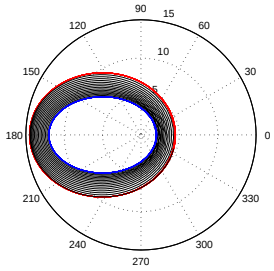

(d) Fifteen Orbits

Figure 7 Optimal Trajectories for Unconstrained Apoapsis Maneuver

APPENDIX B: CONSTRAINED APOAPSIS MANEUVER RESULTS

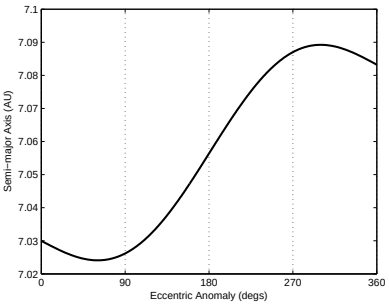

(a) One Orbit

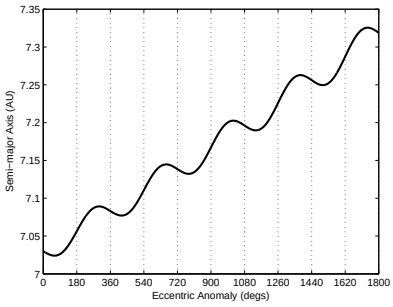

(b) Five Orbits

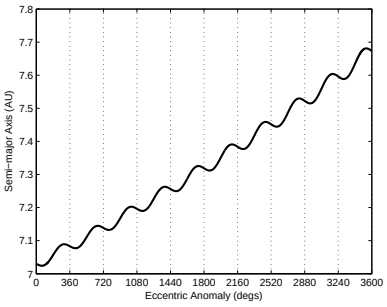

(c) Ten Orbits

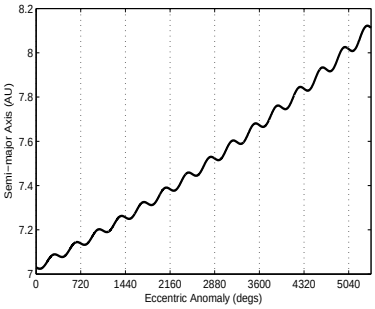

(d) Fifteen Orbits

Figure 8 Semi-Major Axis for Constrained Apoapsis Maneuver

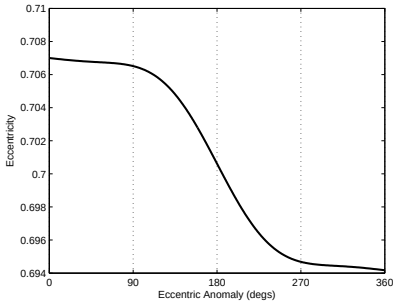

(a) One Orbit

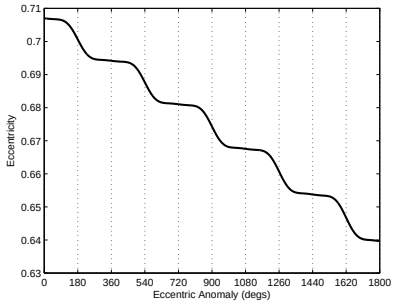

(b) Five Orbits

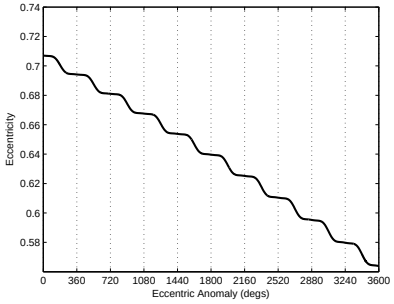

(c) Ten Orbits

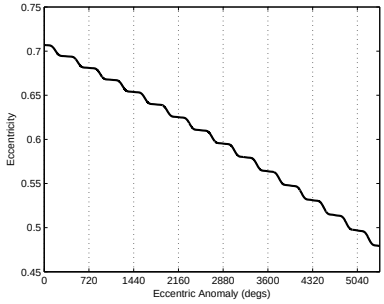

(d) Fifteen Orbits

Figure 9 Eccentricity for Constrained Apoapsis Maneuver

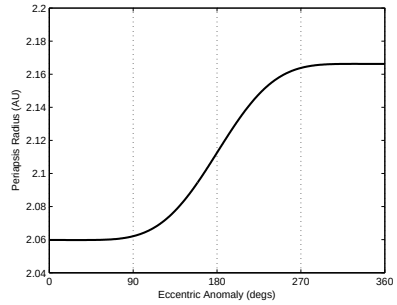

(a) One Orbit

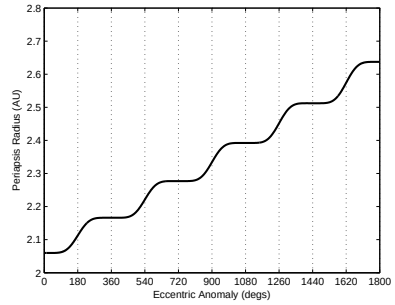

(b) Five Orbits

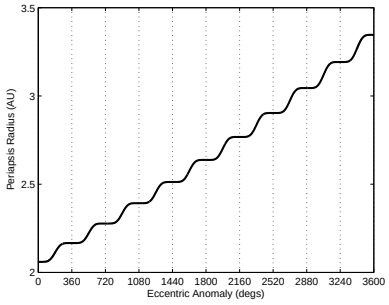

(c) Ten Orbits

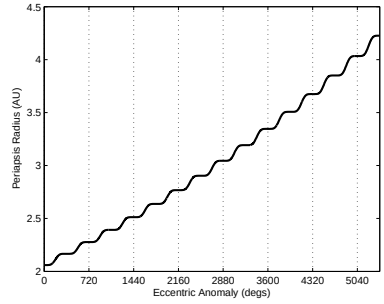

(d) Fifteen Orbits

Figure 10 Periapsis Radius for Constrained Apoapsis Maneuver

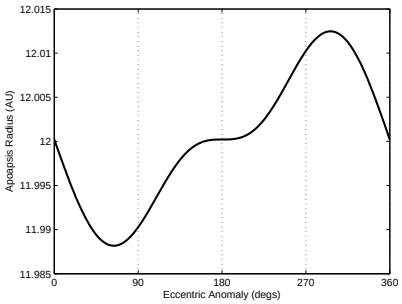

(a) One Orbit

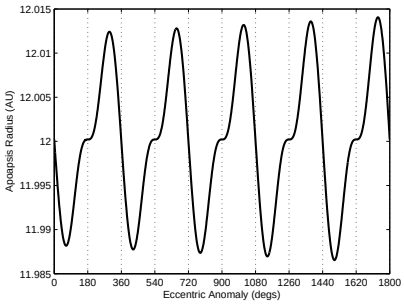

(b) Five Orbits

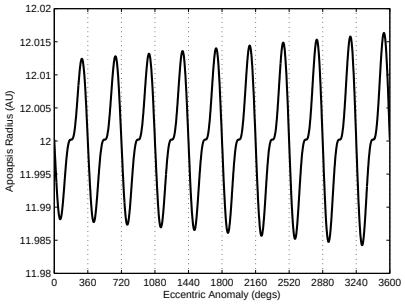

(c) Ten Orbits

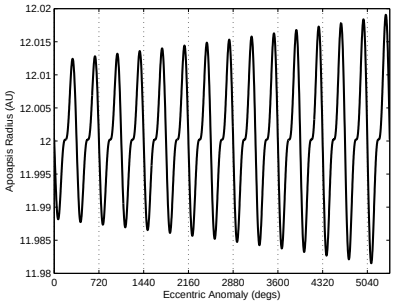

(d) Fifteen Orbits

Figure 11 Apoapsis Radius for Constrained Apoapsis Maneuver

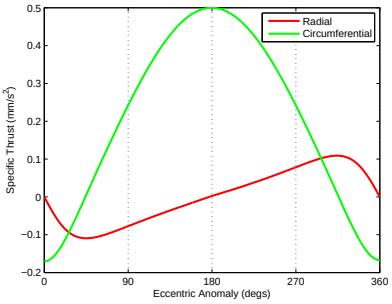

(a) One Orbit

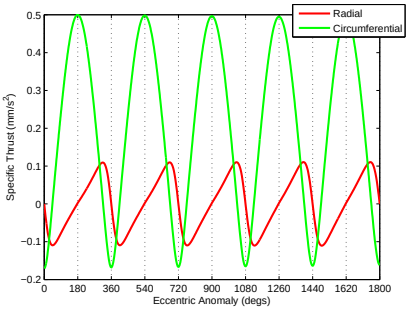

(b) Five Orbits

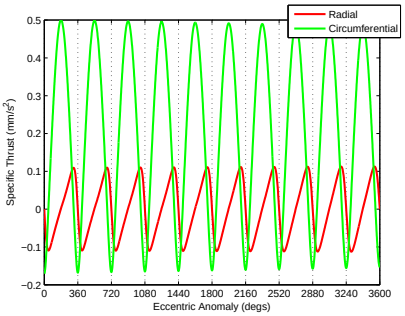

(c) Ten Orbits

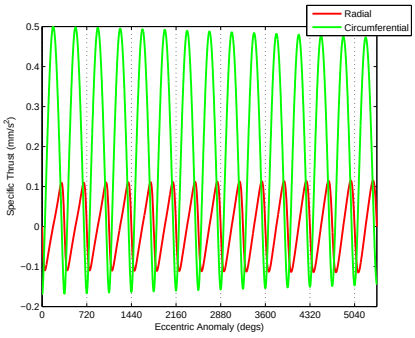

(d) Fifteen Orbits

Figure 12 Specific Thrust for Constrained Apoapsis Maneuver

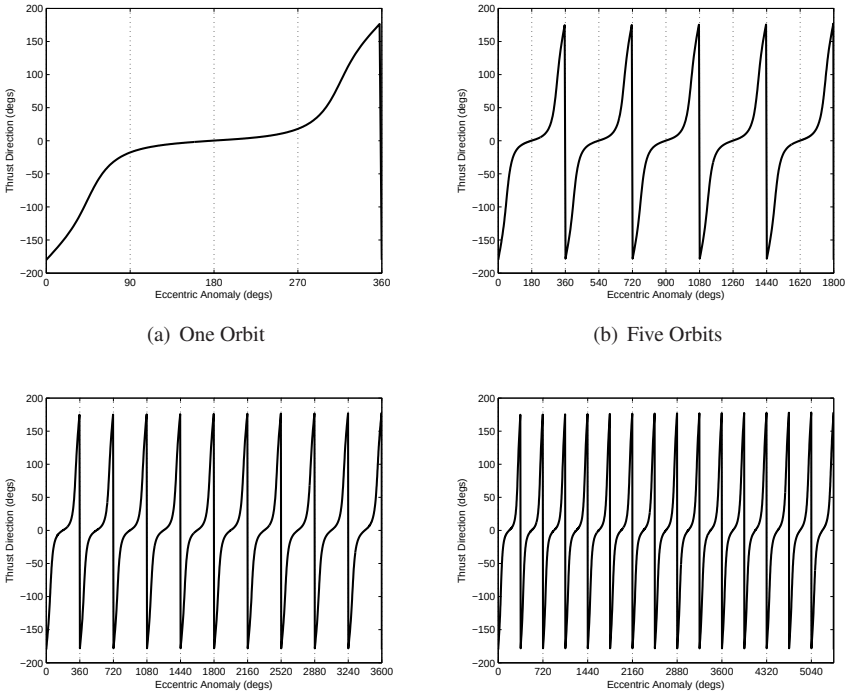

(a) One Orbit

(b) Five Orbits

(c) Ten Orbits

(d) Fifteen Orbits

Figure 13 Thrust Direction for Constrained Apoapsis Maneuver

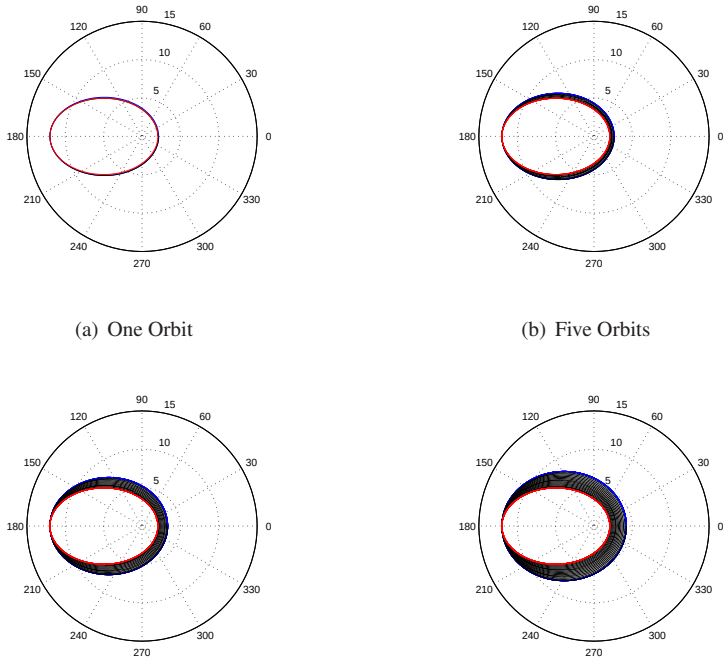

(a) One Orbit

(b) Five Orbits

(c) Ten Orbits

(d) Fifteen Orbits

Figure 14 Optimal Trajectories for Constrained Apoapsis Maneuver